Global Sensitivity Analysis Based on BP Neural Network for Thermal Design Parameters

Yuting Yang,* Liheng Chen,† Yan Xiong,‡ Shijun Li,§ and Xu Meng¶
Changchun Institute of Optics, Fine Mechanics and Physics, Changchun, People's Republic of China

https://doi.org/10.2514/1.T5955

In order to obtain the thermal design parameters that have a great influence on the temperature T of the spectrometer frame, the sensitivity of the thermal design parameters of a balloon-borne spectrometer system was analyzed and calculated by the global sensitivity analysis (GSA) method based on the backpropagation neural network (BPNN) surrogate model. Firstly, the BPNN with 12 selected thermal design parameters as input and temperature T as output was well trained. Then, two kinds of variance-based GSA methods, the Sobol' method and the extended Fourier amplitude sensitivity test (EFAST), were used to calculate the values and ranking results of sensitivity indices of 12 parameters based on the established BPNN. Moreover, the GSA results were verified based on the finite element model of the balloon-borne spectrometer system built by I-DEAS/TMG (software developed by Structural Dynamics Research Corporation for space thermal analysis), which indicates that the BPNN surrogate-model-based GSA is reliable. Finally, the sensitivity calculation accuracy and speed of two methods, the Spearman rank correlation coefficient formula and the GSA method based on BPNN, were compared, and the EFAST method based on the BPNN surrogate model has been proved to have obvious advantages in the reliability and speed of calculation results. Also, the GSA method based on a surrogate model like BPNN is of great significance in the thermal analysis of an optical remote sensor.

Nomenclature

A_x	=	area of xth surface of pod
A_y	=	contact area between two components in the spectrometer system
c_{fr}	=	specific heat capacity of the spectrometer frame
c_m	=	complex coefficient
c_n	=	specific heat capacity of the nth system components
c_{po}	=	specific heat capacity of pod
$D(Y)$	=	total variance of function Y
D_i	=	variance of model output caused by X_i
$D_{\sim i}$	=	variance of model output caused by other parameters besides parameter X_i
E_{e}	=	average infrared radiation intensity of the earth
E_I	=	higher order EFAST sensitivity indices
E_j	=	first order EFAST sensitivity indices of X_i
E_j^T	=	total order EFAST sensitivity indices of X_i
E_{r}	=	average reflection intensity of the earth to the solar radiation
F_x	=	angle coefficient of internal heat source to xth internal surface of pod
$G_\omega(s)$	=	transformation function
h_x	=	average convective heat transfer coefficient of the xth surface of pod
K_y	=	thermal conductivity between two components in the spectrometer system
M_A, M_B, and M_p	=	sample matrices
m_{fr}	=	mass of the spectrometer frame
m_n	=	mass of the nth system components
m_{po}	=	mass of pod
N	=	number of samples
p	=	number of thermal design parameters
Q_{cx}	=	value of heat conducted from the internal heat source to the xth surface of pod
Q_{rx}	=	value of radiation heat transferred from the internal heat source to the xth surface of pod
Q_y	=	value of heat generated by one single internal heat source in pod
Q_1	=	value of heat conduction between pod and electrical box
Q_2	=	value of external heat absorbed by pod
Q_3	=	value of heat generated by all of the internal heat source in pod
Q_4	=	value of aerodynamic heat absorbed by pod
Q_5	=	value of convective heat transfer between pod and atmosphere environment
Q_6	=	value of radiation heat transfer between pod and atmosphere environment
Q_7	=	value of internal energy variation of spectrometer system
q_{ahx}	=	aerodynamic heat flux of xth external surface of pod
R_{DZ}	=	thermal resistance between two mounting surfaces
R_{1y}	=	conduction thermal resistance of the internal components of the spectrometer system
R_{2y}	=	contact thermal resistance between two components in the spectrometer system
S	=	solar constant
S_i	=	first order Sobol' indices of X_i
S_i^{T}	=	total order Sobol' indices of X_i
s	=	scalar variable
T	=	temperature of the spectrometer frame

Received 13 November 2019; revision received 16 July 2020; accepted for publication 30 August 2020; published online 8 December 2020.

*Master Degree Candidate, Thermal Control Group; also University of Chinese Academy of Sciences, 10049 Beijing, People's Republic of China; yytciomp1206@163.com.

†Associate Professor, Thermal Control Group; also University of Chinese Academy of Sciences, 10049 Beijing, People's Republic of China; chenliheng3@163.com (Corresponding Author).

‡Ph.D. Candidate, Thermal Control Group; also University of Chinese Academy of Sciences, 10049 Beijing, People's Republic of China; xiongyan16@mails.ucas.ac.cn.

§Ph.D. Candidate, Thermal Control Group; also University of Chinese Academy of Sciences, 10049 Beijing, People's Republic of China; 1228666705@qq.com

¶Master Degree Candidate, Thermal Control Group; also University of Chinese Academy of Sciences, 10049 Beijing, People's Republic of China; 2378406944@qq.com.

T_{ox} = average temperature of xth external surface of pod
T_D = temperature of the mounting surface of electrical box
T_y = average surface temperature of the internal heat source
T_Z = temperature of the mounting surface of pod
T_e = atmospheric temperature
V = total variance of the model output
V_i = model output variance caused by the parameter X_i
X = set of 12 thermal design parameters
X_1/λ = thermal conductivity of pod
X_2/ε_{1x} = emissivity of external surface of pod
X_3/α_{sx} = solar absorption coefficient of external surface of pod
X_4/ε_{2x} = emissivity of internal surface of pod
X_5/R_1 = thermal resistance between CCD and spectrometer frame
X_6/R_2 = thermal resistance between eletrical box and pod
X_7/R_3 = thermal resistance at the connection of frame of spectrometer
X_8/K_1 = thermal conductivity between spectrometer frame and pod
X_9/K_2 = thermal conductivity between CCD and pod
X_{10}/h_1 = convective heat transfer coefficient of $+Y$, $-Y$ surface of pod
X_{11}/h_2 = convective heat transfer coefficient of $+X$ surface of pod
X_{12}/h_3 = convective heat transfer coefficient of $-X$ surface of pod
x_j = parameter sampling vector
$x_{[j]}$ = triangular-shaped vector
Y = output of BP neural network
α_{sx} = solar absorption coefficient of the xth external surface of pod
ε_{1x} = emissivity of the xth external surface of pod
ε_{2x} = emissivity of xth internal surface of pod
σ = Stefan–Boltzmann constant
φ_{1x}, φ_{2x}, and φ_{3x} = angle factors of pod to the solar radiation, the earth albedo, and the infrared radiation of the earth
ω = angular frequency

I. Introduction

SENSITIVITY analysis (SA) is a crucial step in the model building and result communication process, which has long been a way for system designers to understand the relative importance of parameter inputs in determining the model output [1–3]. SA methods structure into local sensitivity analysis (LSA) and global sensitivity analysis (GSA), and the GSA is to study the effects of simultaneous changes in all design parameters on the overall system, which not only considers the effect of changes in individual parameter values on the system, but also analyzes the influence of the coupling effect generated by the interaction between various parameters on the system [4].

SA for thermal design parameters is of great significance for improving the accuracy of thermal design and reducing resource waste. In the current research of SA for thermal design parameters, the LSA method is generally used. Han [5] performed the LSA of the contact conduction and the position of thermostat on the basis of the established satellite thermal model. Guo [6,7] performed LSA on optical remote sensors in a space environment, and completed thermal design and thermal experiments based on analysis results. In the study of GSA for thermal design parameters, McMenamin [8] used an ANOVA-HDMR (analysis of variance-high dimensional model representation) GSA method to measure the effect that uncertain parameters have on the temperature of Solar X-ray Monitor (SXM), spacecraft battery, and charge coupled devices (CCDs). However, there are few studies on GSA for thermal design parameters. Moreover, there are few studies on the influence of multi-parameter coupling effect on the model output in the existing GSA of thermal design parameters.

In order to introduce the GSA method into the thermal design of an optical remote sensor, this paper adopted the GSA method based on a surrogate model (metamodel) [9–11], which avoids the disadvantage of time-consuming when solving the sensitivity of parameters based on finite element simulators. Based on the thermal design index of the frame temperature T of the balloon-borne spectrometer system, the backpropagation (BP) neural network (BPNN) was adopted to construct the surrogate model of temperature T and 12 selected thermal design parameters. In the selection of GSA method, because variance-based methods have assessed themselves as versatile and effective among the variety of available technologies for sensitivity analysis of model output [12], this paper selected the classical variance-based Sobol' method and extended Fourier amplitude sensitivity test (EFAST) to solve the first and total order effects of the parameters to the temperature observation point. Then, the finite element thermal simulation of a spectrometer system based on I-DEAS/TMG (software developed by Structural Dynamics Research Corporation for space thermal analysis) was completed to verify the correctness of the global sensitivity calculation results of 12 parameters. In addition, the Spearman rank correlation coefficient (SRCC) formula, as a commonly used method for studying the influence of parameters on model output, was introduced in this paper to compare reliability and calculation speed with variance-based GSA methods based on a BPNN surrogate model. The comparison results indicate that the EFAST method based on a BPNN surrogate model has a higher advantage in the reliability of calculation results and calculation speed, and has a higher application value in guiding the thermal design of an optical remote sensor and the modification of a thermal analysis model.

II. Heat Balance Equation of Spectrometer System

A schematic diagram of the balloon-borne spectrometer system is shown in Fig. 1.The balloon-borne spectrometer system consists of a spectrometer, a cube pod, an electrical box, and the high-altitude balloon platform. The spectrometer is mounted inside the pod, which is connected to the electrical box by thermal insulation, with both pod and electrical box mounted on the balloon platform. In order to avoid the interference of airflow when the spectrometer system is flying, the pod is vacuumized internally. The descriptions of the spectrometer system are shown in Table 1.

The typical flying height of the high-altitude balloon is 20 km above sea level. At this altitude, the surface of the pod is affected by external heat fluxes, mainly solar flux from the sun, sunlight reflected off of the earth (albedo), and infrared energy emitted by the earth [13]. The interior of the pod is vacuumed, and the internal heat source can only transfer heat to the pod through thermal conduction and radiation. And then, the pod radiates heat to the atmosphere through surface convection and radiation. Under such a thermal environment, the thermal design goal of the balloon-borne spectrometer system is mainly for temperature T of the spectrometer frame. The lower the temperature T, the better the optical device and CCD working conditions, and the better the imaging quality. According to the thermal environment and temperature index of the spectrometer frame, the schematic diagram of the thermal control of the spectrometer system is shown in Fig. 2.

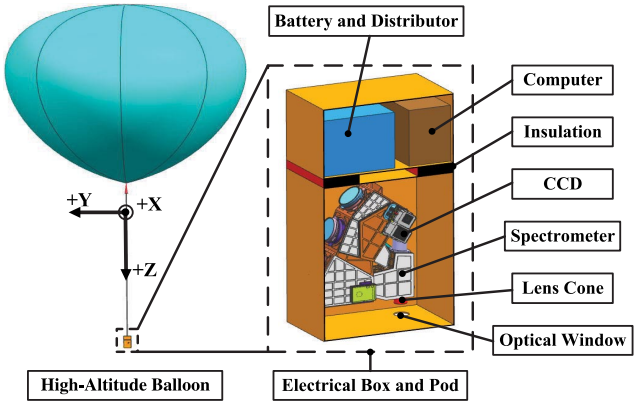

Fig. 1 Schematic of the balloon-borne spectrometer system.

Table 1 Descriptions of spectrometer system

Items	Description
Working time	8 a.m. to 2 p.m., Beijing time Ascent phase: 1 h, level flight: 4 h, landing phase: 1 h
Working latitude	41.7 deg north latitude
Level flight altitude/ Atmospheric ambient temperature	20 km/ − 56.5°C
CCD power	15 W
System heating power	≤200 W
Temperature index for spectrometer frame	Maintaining −5 ± 2°C for more than 3 h within 5 h (Regardless of landing phase)

According to Fig. 2 and the law of conservation of energy, the heat balance equation for the balloon-borne spectrometer system was established as Eq. (1):

$$\begin{cases} Q_1 + Q_2 + Q_3 + Q_4 = Q_5 + Q_6 + Q_7 \\ Q_1 = \dfrac{T_D - T_Z}{R_{\mathrm{DZ}}} \\ Q_2 = \sum(\alpha_{\mathrm{sx}} \mathrm{S}\varphi_{1x} + \alpha_{\mathrm{sx}} E_{\mathrm{r}}\varphi_{2x} + \varepsilon_{1x} E_{\mathrm{e}}\varphi_{3x})A_x \\ Q_3 = \sum Q_y \\ Q_4 = \sum q_{\mathrm{ahx}} A_x \\ Q_5 = \sum h_x A_x (T_{\mathrm{ox}} - T_e) \\ Q_6 = \sum \varepsilon_{1x}\sigma A_x (T_{\mathrm{ox}}^4 - T_e^4) \\ Q_7 = m_1 c_1 \dfrac{\Delta T_1}{\Delta\tau} + \cdots + m_{\mathrm{fr}} c_{\mathrm{fr}} \dfrac{\Delta T}{\Delta\tau} + \cdots + m_n c_n \dfrac{\Delta T_n}{\Delta\tau} \end{cases} \tag{1}$$

where Q_1 is the value of heat conduction between pod and electrical box; T_D and T_Z are the temperatures of the mounting surface of the electrical box and the pod, respectively; R_{DZ} is the thermal resistance between the two mounting surfaces; Q_2 is the value of external heat absorbed by the pod; α_{sx} is the solar absorption coefficient of the xth external surface of the pod; S is the solar constant; E_{r} is the average reflection intensity of the earth to the solar radiation; ε_{1x} is the emissivity of the xth external surface of the pod; E_{e} is the average infrared radiation intensity of the earth; φ_{1x}, φ_{2x}, and φ_{3x} are the angle factors of the xth external surface of the pod to the solar radiation, the earth albedo, and the infrared radiation of the earth, respectively; A_x is the area of the xth surface of the pod; Q_3 is the value of heat generated by all of the internal heat sources in the pod; Q_y is the value of heat generated by one single internal heat source in the pod; Q_4 is the value of aerodynamic heat absorbed by the pod; q_{ahx} is the aerodynamic heat flux of the xth external surface of the pod; Q_5 is the value of convective heat transfer between the pod and the atmosphere environment; h_x is the average convective heat transfer coefficient of the xth surface of the pod; T_{ox} is the average temperature of the xth external surface of the pod; T_e is the atmospheric temperature; Q_6 is the value of radiation heat transfer between the pod and the atmosphere environment; Q_7 is the value of internal energy variation of the spectrometer system; m_n is the mass of the nth system components; c_n is the specific heat capacity of the nth system components; m_{fr} and c_{fr} are the mass and specific heat capacity of the spectrometer frame, respectively; T is the temperature of the spectrometer frame; $(\Delta T_n/\Delta\tau)$ is the temperature change rate of the nth system components; and $\Delta T/\Delta\tau$ is the temperature change rate of the spectrometer frame.

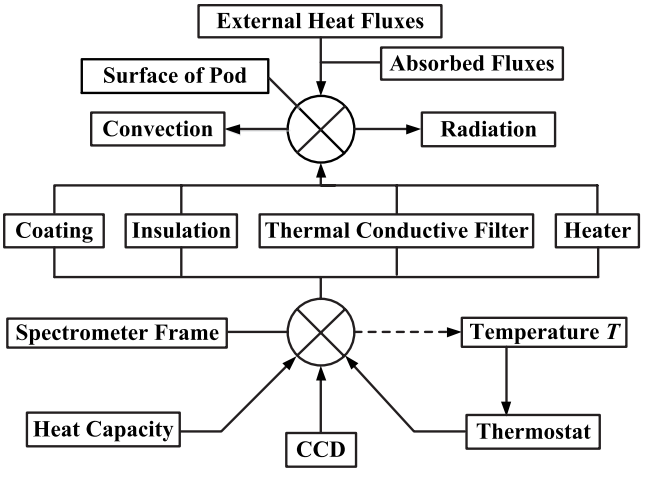

Fig. 2 Thermal control schematic of the spectrometer system.

III. Parameter Selection for GSA

According to Eq. (1), parameters related to the temperature T of the spectrometer frame need to be selected for GSA. According to the heat balance equation, the expression of temperature T can be obtained by inverse solution, which is a complex function of multiple parameters and can be written as an abstract function as Eq. (2):

$$T = f(R_{\mathrm{DZ}}, \alpha_{\mathrm{sx}}, \varphi_{1x}, \varphi_{2x}, \varphi_{3x}, \varepsilon_{1x}, A_x, q_{\mathrm{ahx}}, h_x, T_{\mathrm{ox}}, T_e, m_n, c_n, \cdots) \tag{2}$$

In Eq. (2), the external surface temperature of the pod T_{ox} is also a complex function affected by many parameters, which can be written as follows:

$$T_{\mathrm{ox}} = \sum \frac{Q_{\mathrm{cx}}}{\sum R_{1y} + \sum R_{2y} + \sum \frac{1}{K_y A_y}} + \sum \sqrt[4]{T_y - \frac{Q_{\mathrm{rx}}}{\varepsilon_{2x}\sigma F_x}} + \frac{Q_1 + Q_2 + Q_4 - Q_5 - Q_6}{c_{\mathrm{po}} m_{\mathrm{po}}} \tag{3}$$

where Q_{cx} is the value of heat conducted from the internal heat source to the xth surface of pod, R_{1y} is the conduction thermal resistance of the internal components in the spectrometer system, R_{2y} is the contact thermal resistance between two components in the system, K_y is the thermal conductivity between two components, A_y is the contact area between two components in the system, Q_{rx} is the value of radiation heat transferred from the internal heat source to the xth surface of the pod, T_y is the average surface temperature of the internal heat source, ε_{2x} is the emissivity of the xth internal surface of the pod, F_x is the angle coefficient of the internal heat source to the xth internal surface of the pod, and c_{po} and m_{po} are the specific heat capacity and mass of pod, respectively.

From Eqs. (2) and (3), the parameters affecting the temperature T can be obtained. In terms of selecting the parameters for GSA, the selection criteria are firstly determined according to whether the parameters can be changed arbitrarily in the actual spectrometer system. Due to the limitations of the system's optical structure, a large number of parameters affecting the temperature T cannot be changed. Then, among the parameters that can be changed, the important parameters that have either a direct or an indirect relationship with the temperature T should be mainly selected:

1) For the selection of adjustable parameters that directly affect the temperature T, the parameters related to thermal radiation and heat conduction need to be selected due to the vacuum treatment in the pod. In the selection of radiation parameters, only the internal surface emissivity ε_{2x} of the pod was selected due to the fixed surface radiation characteristics of the spectrometer. In terms of the selection of thermal conduction parameters, because CCD is the main internal heat source, the surface of the spectrometer is the main heat sink, and the frame temperature of the spectrometer is the main design goal, the thermal resistance/thermal conductivity between CCD and spectrometer and between spectrometer and pod were screened out for GSA, taken as R_1 and K_1.

2) For the selection of parameters that indirectly affect the temperature T, the parameters affecting the heat sink temperature of the pod T_{ox} were mainly selected. According to Eq. (3), T_{ox} is affected by the external heat fluxes, internal heat source, and surface heat dissipation capacity of the pod. Therefore, the surface radiation parameters α_{sx} and ε_{1x} and the convective heat transfer coefficients h_x of the pod were selected first. Then, the two heat sources of CCD and the electrical box both have influence on the pod temperature in the way of heat conduction. Therefore, the thermal conductivity/thermal resistance between CCD and pod and between electrical box and pod were screened out for GSA, taken as K_2 and R_2. In order to consider the importance of the thermal conductivity of the pod on the temperature of the spectrometer frame, GSA was also carried out for the thermal conductivity λ of the pod by setting the value range of λ to 100–400, taking the thermal conductivity of aluminum alloy as the lower limit and the thermal conductivity of copper as the upper limit. In addition, in order to verify the influence of the thermal resistance of the spectrometer frame structure on its temperature level, thermal resistance at the connection of the frame R_3 was also involved in the GSA.

After summarizing the preceding parameters and recoding them to X_i, 12 parameters for GSA are obtained, and the detailed descriptions of 12 parameters for GSA are shown in Table 2.

In order to solve the sensitivity indices of the selected parameters, it is necessary to establish the mathematical relationship between the input (12 parameters) and output (temperature T) of the model. First, according to the three-dimensional model and thermal control scheme of the spectrometer system, I-DEAS/TMG was used to establish the finite element model of the balloon-borne spectrometer system. The finite element model of the system is shown in Fig. 3. This model has 4606 elements, 4874 nodes, and 56 thermal couplings.

After the finite element model was built, the simulation results of spectrometer-frame temperature T can be obtained. By adjusting some or all of the parameters in the model, the variation of temperature T can be obtained, that is, the local sensitivity of the parameters. Figure 4 shows the change of temperature T when some parameters are changed individually.

The analysis results of LSA include the partial derivative information of temperature T to the selected parameter, and explain the influence mode and degree of the parameter to temperature T. However, in fact, the local sensitivity cannot distinguish the coupling effect of a single parameter with other parameters at temperature T, so GSA is necessary for temperature T and 12 parameters.

Table 2 Descriptions of 12 thermal design parameters for GSA

Parameter	Description	Range
X_1/λ	Thermal conductivity of pod, W/(m · K)	100–400
X_2/ε_{1x}	Emissivity of external surface of pod	0.01–1
X_3/α_{sx}	Solar absorption coefficient of external surface of Pod	0.01–1
X_4/ε_{2x}	Emissivity of internal surface of pod	0.01–1
X_5/R_1	Thermal resistance between CCD and spectrometer frame, K/W	0.01–50
X_6/R_2	Thermal resistance between electrical box and pod, K/W	0.01–50
X_7/R_3	Thermal resistance at the connection of frame of spectrometer, K/W	0.01–10
X_8/K_1	Thermal conductivity between spectrometer frame and pod, W/(m^2 · K)	100–1000
X_9/K_2	Thermal conductivity between CCD and pod, W/(m^2 · K)	100–1000
X_{10}/h_1	Convection heat transfer coefficient of $+Y$, $-Y$ surface of pod, W/(m^2 · K)	0.1–10
X_{11}/h_2	Convection heat transfer coefficient of $+X$ surface of pod, W/(m^2 · K)	0.1–10
X_{12}/h_3	Convection heat transfer coefficient of $-X$ surface of pod, W/(m^2 · K)	0.1–10

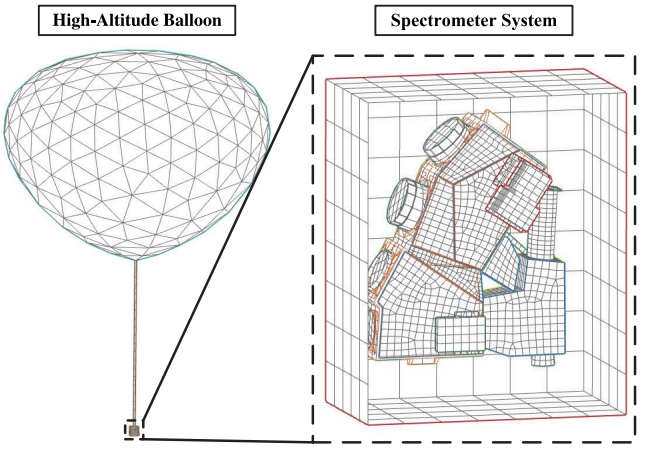

Fig. 3 Finite element model of balloon-borne spectrometer system.

IV. Variance-Based GSA for Thermal Design Parameters

In the variance-based GSA of parameters, it is usually necessary to sample a large number of parameters in their value space and get the corresponding function output, and then calculate the global sensitivity indices of parameters based on the sampling results. However, due to the high time-consumption of finite element model simulation, when the GSA method such as the Sobol' method was directly used in this model to calculate the convergent sensitivity indices, the calculation time cost would be enormous. In order to improve the calculation efficiency of GSA, a surrogate model (or metamodel) is often used in the GSA of a complex model. Among many surrogate models, an artificial neural network is often used in the calculation of the sensitivity of parameters because of its good nonlinear fitting ability [14,15]. Therefore, this paper selected BP neural network (BPNN) as the surrogate model to represent the mathematical relationship between temperature T and 12 thermal design parameters to replace the finite element model. Based on established BPNN, the sensitivity calculation of 12 parameters was completed by using the variance-based GSA methods: Sobol' method and extended Fourier amplitude sensitivity test (EFAST) method.

A. Establishment of BPNN

BPNN is a multilayer feedforward neural network [16]. Figure 5 shows the architecture of BPNN.

The topological structure of BPNN consists of three layers of neurons: input layer, hidden layer, and output layer. The input layer and output layer have neurons that represent the input and output variable, respectively. The hidden layer has one or more neurons to show nonlinear relations between input and output in the systems [17]. Neurons in one layer are connected to neurons in other layers, and each connection has a corresponding connection weight, which quantitatively describes the connection strength among neurons. Training of BPNN is the process of backpropagating the errors from the output layer toward the input layer. Backpropagation is necessary because the hidden neurons have no target values that can be used, so these neurons must be trained based on errors from the previous layers. The output layer has a target value that is used to compare with the calculated value. As the errors are backpropagated through the neurons, the connection weights are continuously updated. Training will occur until the errors in the weights are adequately small enough to be accepted [18]. After adjusting the connection weights and thresholds continuously to meet the training errors, BPNN can establish an accurate nonlinear mapping relationship between input and output.

In order to establish BPNN with 12 thermal design parameters as input and temperature T as output, a training set should be established. First of all, 12 parameters need to be sampled in their respective value spaces. In order to avoid the nonuniformity of the sampled data sets that cannot cover the entire value space of the parameters, leading to extreme errors in BPNN prediction, this work used the

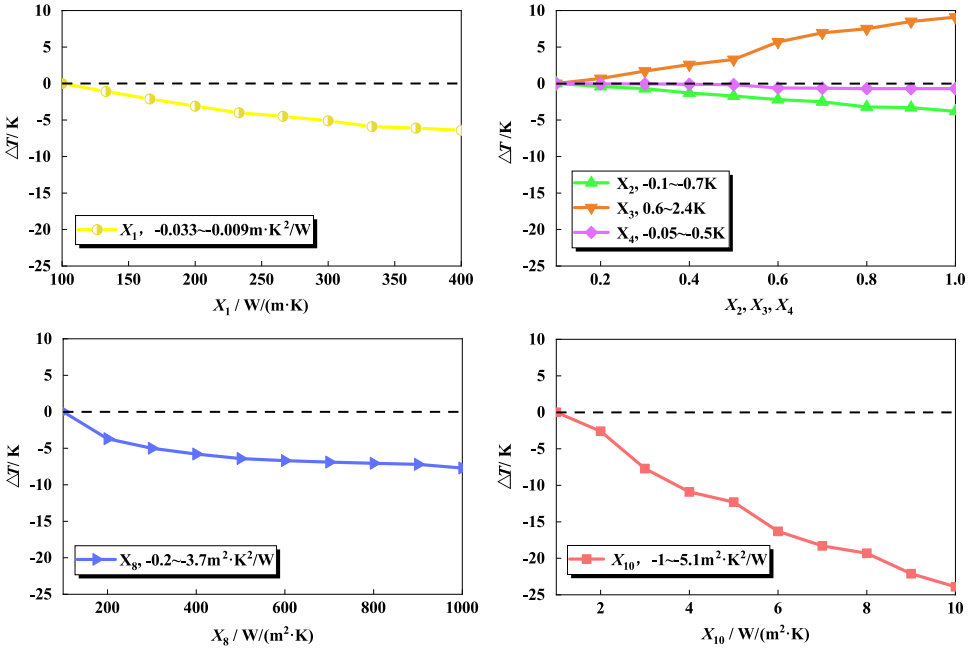

Fig. 4 Local sensitivity of some parameters.

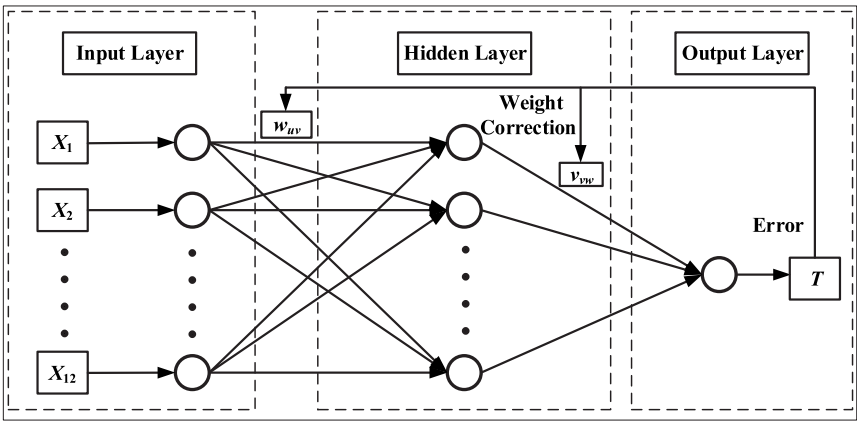

Fig. 5 Architecture of BPNN.

Latin hypercube sampling (LHS) method to obtain the sampling of 12 parameters in their respective value space. By using the LHS method, 12 parameters in Table 1 were sampled 200 times, forming 200 groups of data sets. And then, in order to establish the mathematical relationship between the 12 parameters and the temperature T of the spectrometer frame, according to the finite element model of the spectrometer system, the temperature T corresponding to each group of parameters in the summer solstice was simulated. The simulation parameters of the summer-solstice working condition are shown in Table 3.

Based on the parameter settings in Table 3 and Fig. 6, the sampled data set was substituted into the finite element model, and the corresponding temperature T under summer- solstice working conditions for each set of parameters was obtained. Two hundred sets of parameters and corresponding T constitute the data sets for the training of BPNN, which is shown in Table 4.

In order to obtain BPNN with high fitting accuracy and improve the training and convergence speed of the model, this work used the BP neural network toolbox of MATLAB [19], and the "tansig" and "purelin" functions were used as the activation functions of the hidden and output layers, respectively. In the training process, 80% of the original samples in Table 2 were used for training, 10% were used to validate the generality of the network, and the remaining 10% were used for testing. The number of hidden layer nodes and the learning rate were carefully chosen to overcome the overfitting and underfitting problems, taking 15 and 0.1, respectively. After training for 11 iterations, the mean square error of BPNN training is 2.66e-6, which is less than the preset training goal of 1e-4, and BPNN training was completed and the 12-5-1 network training was obtained. Figure 7 shows the regression of BPNN training. The regression situation of BPNN indicates that the established BPNN can absolutely reflect the functional relationship between temperature T and

Table 3 Description of the simulation parameters under the summer solstice working condition

Item	Description
Solar constant	1323 W/m^2
Average external thermal fluxes of each surface	$+Z$: 684.3 W/m^2, $+Y$: 426.2 W/m^2, $-Y$: 315.7 W/m^2, $+X$: 553.1 W/m^2, $-X$: 553.2 W/m^2
System initial temperature	25°C
Atmospheric temperature and pressure	Shown in Fig. 6
CCD working time	Whole process
Active heating measures	Not work
Time of simulation for generating data sets	1 h for ascent phase

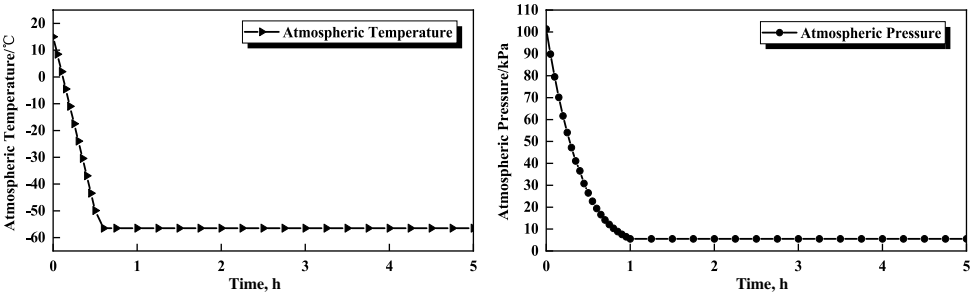

a) Atmospheric temperature b) Atmospheric pressure

Fig. 6 Curve of atmospheric temperature and pressure.

Table 4 Samples of partial data sets for BPNN training

Order	X_1	X_2	X_3	X_4	X_5	X_6	X_7	X_8	X_9	X_{10}	X_{11}	X_{12}	T/K
1	106.48	0.11	0.03	0.14	31.48	26.91	4.29	748.11	102.67	2.85	6.82	7.63	270.45
2	170.85	0.35	0.44	0.25	32.67	48.64	8.29	411.63	971.93	7.92	0.07	4.24	264.03
3	211.42	0.74	0.91	0.89	5.73	1.31	6.21	699.72	948.64	8.88	5.01	0.08	263.75
4	253.93	0.08	0.88	0.41	40.64	3.86	0.75	599.73	395.73	8.21	1.48	5.47	268.51
	117.18	0.01	0.36	0.61	8.16	39.27	5.68	302.18	719.21	6.27	5.11	4.91	267.64
…	…	…	…	…	…	…	…	…	…	…	…	…	…
197	166.93	0.95	0.02	0.71	38.53	29.23	2.48	902.88	455.26	4.79	2.94	1.01	262.45
198	105.71	0.14	0.07	0.74	6.54	25.94	0.45	930.64	90.67	6.69	7.21	9.48	260.75
199	236.41	0.02	0.58	0.88	1.08	13.32	9.55	344.59	637.23	7.91	5.15	10.91	262.25
200	102.39	0.09	0.67	0.84	28.62	35.58	6.62	420.05	884.5	8.37	9.72	3.91	263.45

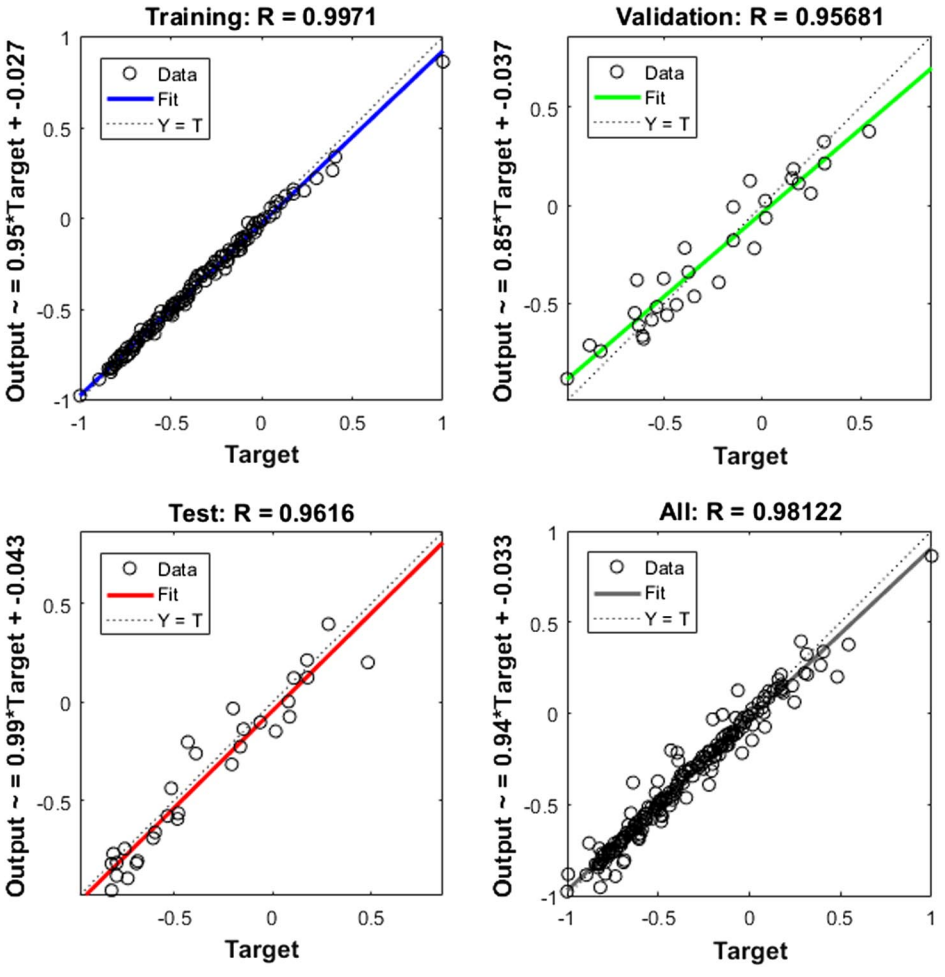

Fig. 7 Regression situation of established BPNN.

12 parameters, and can be used for the GSA of parameters based on this BPNN.

B. Sobol' Method

The Sobol' method [20] is a Monte Carlo method based on variance. The main idea of sensitivity calculation by the Sobol' method is to decompose the function $f(x)$ into the sum of 2^p incremental terms, and then obtain the sensitivity indices of each parameter by sampling and calculating the total variance and each partial variance of the influence of parameters on the model. In practical engineering applications, because of the complexity of the actual function model, it is generally impossible to calculate all variances. Therefore, Monte Carlo integration is often used to estimate the variance of the output of the model. When the sample size of the model parameters is large enough, the calculated results nearly approximate the analytical solution. In this work, the GSA for 12 thermal design parameters was performed by using the Sobol' method based on Monte Carlo integration. The Sobol' indices calculation process is as follows:

1. First, abstract BPNN into the following abstract functions:

$$Y = f(X) \tag{4}$$

where $X = \{X_1, \ldots, X_{12}\}$ is the set of 12 thermal design parameters and Y is the output of BPNN (i.e., temperature T).

2. Afterward, an original sampling matrix $N \times 24$ was obtained by carrying out quasi–Monte Carlo sampling for creating independent samples. After splitting the original sampling matrix into two halves, sampling matrix M_A ($N \times 12$) and resampling matrix M_B ($N \times 12$) were obtained, respectively, as shown in Eq. (5):

$$M_A = \begin{bmatrix} X_{11} & X_{12} & \cdots & X_{1p} \\ X_{21} & X_{22} & \cdots & X_{2p} \\ \vdots & \vdots & & \vdots \\ X_{N1} & X_{N2} & \cdots & X_{Np} \end{bmatrix}, \quad M_B = \begin{bmatrix} X'_{11} & X'_{12} & \cdots & X'_{1p} \\ X'_{21} & X'_{22} & \cdots & X'_{2p} \\ \vdots & \vdots & & \vdots \\ X'_{N1} & X'_{N2} & \cdots & X'_{Np} \end{bmatrix} \tag{5}$$

where X_{zi} and X'_{zi} are the normalized element in the sampling and resampling matrix obtained by sampling 12 parameters in their respective value spaces twice; z represents the number of groups of sampling parameters, $z \in \{1, 2, \ldots, N\}$; N is the number of samples, $N = 20{,}000$ (the greater the value of N, the better the convergence of the result of parameter sensitivity calculation); i takes 1 to p to represent p parameters from X_1 to X_p; and p is the number of thermal design parameters, $p = 12$. On the basis of sample M_A and M_B, the remaining 12 new sample matrices were resampled:

$$\left.\begin{aligned} M_1 &= \begin{bmatrix} X_{11} & X'_{12} & \cdots & X'_{1p} \\ X_{21} & X'_{22} & \cdots & X'_{2p} \\ \vdots & \vdots & & \vdots \\ X_{N1} & X'_{N2} & \cdots & X'_{Np} \end{bmatrix}, \cdots, \\ M_p &= \begin{bmatrix} X'_{11} & X'_{12} & \cdots & X_{1p} \\ X'_{21} & X'_{22} & \cdots & X_{2p} \\ \vdots & \vdots & & \vdots \\ X'_{N1} & X'_{N2} & \cdots & X_{Np} \end{bmatrix} \end{aligned}\right\} \tag{6}$$

where the first column of M_1 is from the first column of M_A, and the column p of M_p is from the column p of M_A, whereas the remaining entries are taken from M_B.

3. Thirdly, a total of 280,000 sets of parameters in 14 sample matrices obtained by sampling were substituted into the BPNN, and the function value Y, which is the corresponding predicted temperature T to each set of parameters, was calculated.

4. Finally, the Sobol' indices of each thermal design parameter X_i were calculated by substituting the function values obtained in step 2 into Eqs. (7–12):

$$\hat{D}(Y) = \frac{1}{2N-1}\sum_{j=1}^{N}\Big[f^2\Big(X_{z1}, X_{z2}, \cdots, X_{zp}\Big) + f^2\Big(X'_{z1}, X'_{z2}, \cdots, X'_{zp}\Big)\Big] - \hat{f}_0^2 \tag{7}$$

$$\hat{f}_0^2 = \frac{1}{N}\sum_{z=1}^{N}\Big[f\Big(X_{z1}, X_{z2}, \cdots, X_{zp}\Big) \times f\Big(X'_{z1}, X'_{z2}, \cdots, X'_{zp}\Big)\Big] \tag{8}$$

$$\hat{D}_i = \frac{1}{N-1}\sum_{z=1}^{N}\Big[f\Big(X_{z1}, X_{z2}, \cdots, X_{zp}\Big) \times f\Big(X'_{z1}, X'_{z2}, \cdots, X'_{z(i-1)}, X_{zi}, X'_{z(i+1)}, \cdots, X'_{zp}\Big)\Big] - \hat{f}_0^2 \tag{9}$$

$$\hat{D}_{\sim i} = \frac{1}{N-1}\sum_{z=1}^{N}\Big[f\Big(X'_{z1}, X'_{z2}, \cdots, X'_{zp}\Big) \times f\Big(X'_{z1}, X'_{z2}, \cdots, X'_{z(i-1)}, X_{zi}, X'_{z(i+1)}, \cdots, X'_{zp}\Big)\Big] - \hat{f}_0^2 \tag{10}$$

$$S_i = D_i / D(Y) \tag{11}$$

$$S_i^{\mathrm{T}} = 1 - D_{\sim i} / D(Y) \tag{12}$$

where $D(Y)$ is the total variance of function Y, D_i is the variance of model output caused by X_i, $D_{\sim i}$ is the variance of model output caused by other parameters besides parameter X_i, $\hat{\cdot}$ represents the estimated value, S_i are the first order Sobol' indices of the ith parameter, and S_i^{T} are the total order Sobol' indices of the ith parameter.

In the process of parameter sampling, this work used a quasi random-number generator in MATLAB, qrandstream based on the Sobol' method, to construct 12 parameters' quasi–Monte Carlo sampling. Based on this random number generator, each parameter sampling result is a kind of probability density distribution with approximate uniform distribution. Figure 8 shows the probability distribution of some parameters after 20,000 times of sampling, and the probability distribution law of other parameters not given in Fig. 8 is consistent with that of parameters in the figure.

According to the preceding formula and sampling results, the first and total order Sobol' indices of the 12 thermal design parameters were obtained by programming with the established BPNN. Table 5 shows the first and total order Sobol' indices of 12 thermal design parameters and the difference $S_i^T - S_i$ between them. The value of this difference reflects the influence of the ith parameter coupled with other parameters on the temperature T. The ranking results of 12 parameters' Sobol' indices are shown in Fig. 9.

From Table 5 and Fig. 9, it can be seen that the first and total order Sobol' indices of X_{10}, X_3, X_5, X_2, and X_6 are the largest, all of which exceed 0.05, whereas the others' are almost all lower than 0.05. This result shows that the five parameters X_{10}, X_3, X_5, X_2, and X_6 have a greater impact on temperature T, whereas the other parameters have a relatively small impact. Among all 12 parameters, because the first order Sobol' index of X_1 is equal to 0 (the result of Monte Carlo integration is -0.0011, which is approximately 0, due to the nonnegativity of Sobol' indices), it indicates that X_1 has little effect on the temperature T and is an insensitive parameter to temperature T [21].

In addition, the difference between the total order Sobol' indices and the first order Sobol' indices $S_i^{\mathrm{T}} - S_i$ also reflects the influence of the coupling of a single parameter and other parameters on temperature T. Comparing the $S_i^{\mathrm{T}} - S_i$ values of different parameters in Table 5, it is obvious that the $S_i^{\mathrm{T}} - S_i$ values of X_8, which is lower ranked in first order Sobol' indices, are relatively larger, indicating

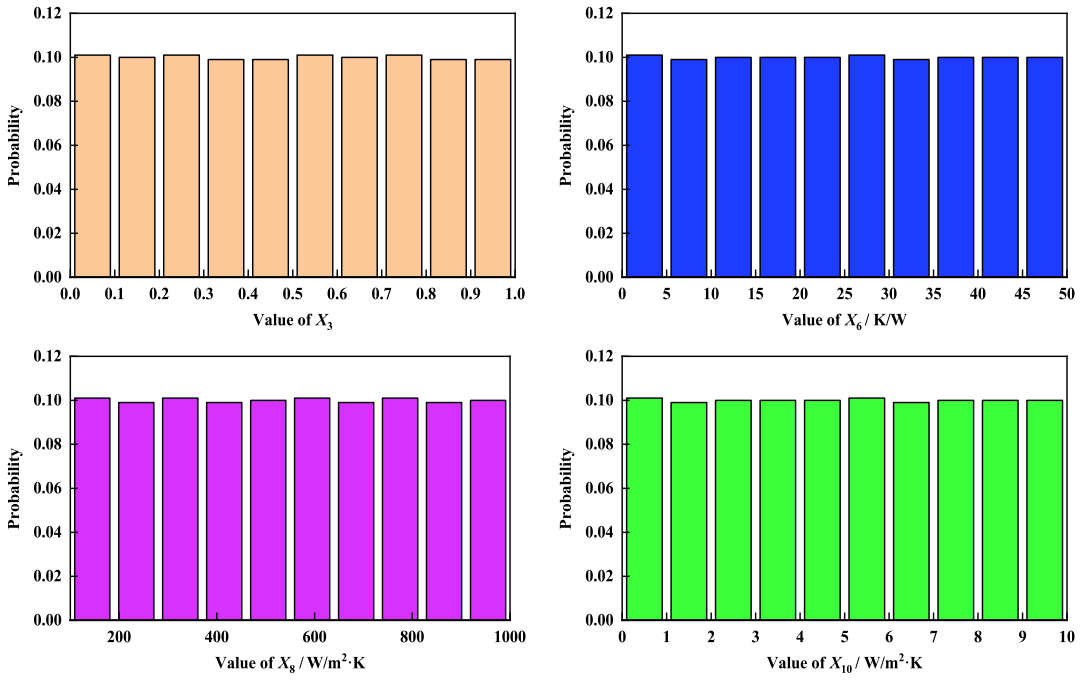

Fig. 8 Probability distribution of some parameters' sampling.

that this parameter needs to be combined with other parameters to affect the temperature T.

Furthermore, this study verified the convergence of Sobol' indices calculated with $N = 20{,}000$. By calculating the Sobol' indices of 12 parameters under a different sampling number N for 100 times respectively, the first and total order Sobol' indices box diagram of 12 parameters with $N = 100$, 1000, 10,000, and 20,000 was obtained, as shown in Fig. 10. It can be seen from Fig. 10 that with the increase of sampling number N, the floating range of the Sobol' index of each parameter gradually decreases. When $N = 20{,}000$, the Sobol' index of each parameter converges to the central value with no intersection with others', which verifies the convergence of Sobol' indices of 12 parameters calculated with $N = 20{,}000$. Afterward, in order to verify the reliability of sensitivity indices calculated by the Sobol' method based on BPNN, further sensitivity calculation and finite element simulation verification are needed.

C. Extended Fourier Amplitude Sensitivity Test

The extended Fourier amplitude sensitivity test (EFAST) is another GSA method based on variance [22]. This method is based on the Fourier amplitude sensitivity test (FAST) method and Sobol' method, and computationally efficient when calculating the sensitivity indices of parameters compared with the Sobol' method. In this section, the sensitivity indices of parameters calculated by the EFAST method was used to verify the calculation results of the Sobol' method. The sensitivity indices' calculation principle of 12 parameters based on the EFAST method is as follows [23]:

1. Firstly, transform the parameter sampling vector x_j into a triangular-shaped vector based on the map $G_\omega(s)$ as:

$$\pi((x_j)) = x_{[j]} = \begin{cases} x_{(2j-1)}, & j \le \dfrac{n+1}{2}, \\ x_{(2(n+1-j))}, & j > \dfrac{n+1}{2}, \end{cases} \qquad j = 1, 2, \ldots, n \tag{13}$$

$$G_\omega(s) = \frac{1}{\pi}\arccos(\cos(2\pi\omega s)) \tag{14}$$

where s is a scalar variable varying over the range $-\pi, \pi$, ω is angular frequency, and $G_\omega(s)$ is the transformation map. The triangular-shaped vector satisfies the following conditions:

$$x_{[j]} \le x_{[j+1]} \text{ if } j \le \frac{n+1}{2}, \quad x_{[j]} \ge x_{[j+1]} \text{ if } j > \frac{n+1}{2} \tag{15}$$

2. Secondly, expand $y = f(x)$ as periodic function $\pi(y)$, and the complex coefficients of the discrete Fourier transform of $\pi(y)$ can be written as:

$$c_m = \sum_{\kappa=1}^{n} (\pi(y))_\kappa \zeta_n^{(\kappa-1)m}, \zeta_n = e^{-2\pi i/n}, m = 0, \pm 1, \pm 2, \ldots, \pm[n/2] \tag{16}$$

where c_m is the complex coefficient of $\pi(y)$. Moreover, the estimate of the first order EFAST sensitivity index is given by:

Table 5 Sobol' indices of 12 thermal design parameters

Parameter	S_i	S_i^T	$S_i^T - S_i$
X_1	0	0.0103	0.0103
X_2	0.0668	0.0836	0.0168
X_3	0.2018	0.2506	0.0488
X_4	0.0027	0.0244	0.0217
X_5	0.0769	0.0988	0.0219
X_6	0.0516	0.0823	0.0307
X_7	0.0016	0.0121	0.0105
X_8	0.0044	0.0561	0.0517
X_9	0.0090	0.0185	0.0095
X_{10}	0.4440	0.4981	0.0541
X_{11}	0.0258	0.0532	0.0274
X_{12}	0.0024	0.0155	0.0131
Sum	0.887	1.2035	0.3165

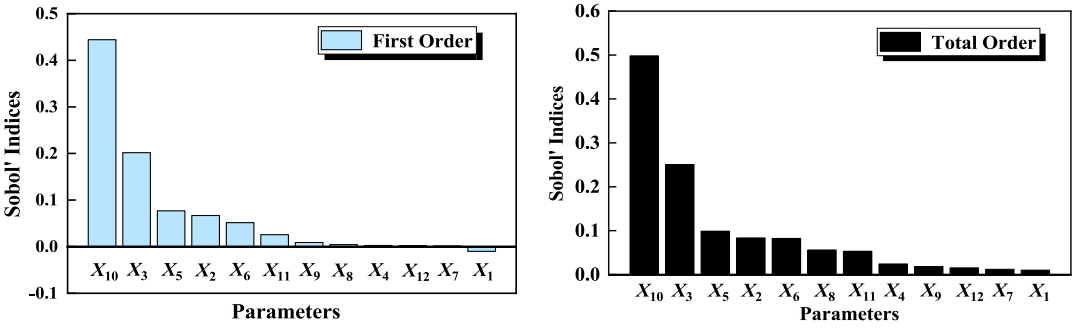

a) First Order b) Total Order

Fig. 9 First and total order Sobol' indices of 12 parameters.

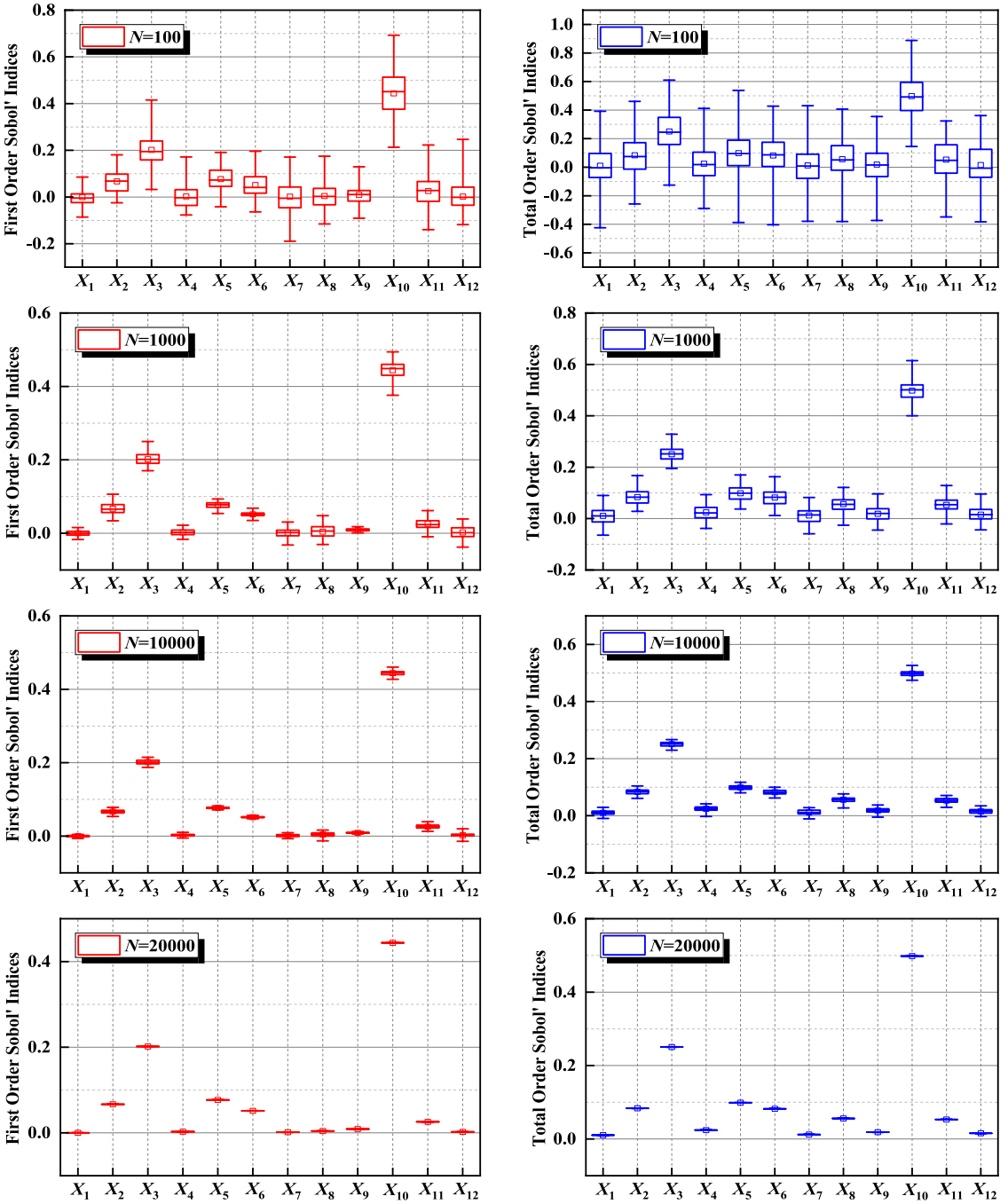

Fig. 10 Convergence verification of Sobol' indices results.

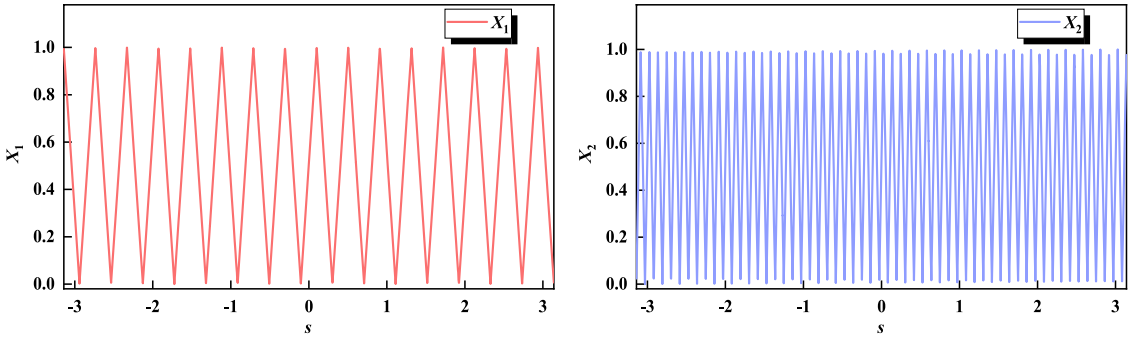

a) X_1 b) X_2

Fig. 11 Periodic sampling of some parameters.

Table 6 EFAST sensitivity indices of 12 thermal design parameters

Parameter	E_j	E_j^{T}	$E_j^{\mathrm{T}} - E_j$
X_1	0	0.0094	0.0094
X_2	0.0706	0.0818	0.0112
X_3	0.1989	0.2544	0.0555
X_4	0.0013	0.0314	0.0301
X_5	0.0712	0.0935	0.0223
X_6	0.0489	0.0807	0.0318
X_7	0.0003	0.0132	0.0129
X_8	0.0035	0.0572	0.0537
X_9	0.0077	0.0156	0.0079
X_{10}	0.4217	0.4792	0.0575
X_{11}	0.0219	0.0496	0.0277
X_{12}	0.0009	0.0207	0.0198
Sum	0.8469	1.1867	0.3398

$$\hat{E}_j = \frac{\sum_{m=1}^{M} |c_m|^2 + |c_{-m}|^2}{\sum_{m\neq 0}^{M} |c_m|^2} = 2\frac{\sum_{m=1}^{M} |c_m|^2}{\sum_{m\neq 0}^{M} |c_m|^2} \tag{17}$$

3. Thirdly, for calculating the higher order EFAST sensitivity indices E_I, on the premise that the parameter group I ($I = \{x_1, \ldots, x_\ell\}, \ell \geq 2$) and the nonlinear correlated sets of angular frequencies ω ($\omega_1, \omega_2, \ldots, \omega_l$) of each column vector are given, the estimate for E_I can also use the complex coefficients c_m of a discrete Fourier transform to express:

$$\hat{E}_I = \frac{\sum_{m\in\Omega_i} |c_m|^2}{\sum\limits_{m\neq 0} |c_m|^2} \tag{18}$$

where $\Omega_I = \{\pm m_1\omega_1 \pm m_2\omega_2 \pm \ldots \pm m_\ell\omega_\ell, m_\ell \in \{1, 2, \ldots, M\}\}$.

4. Then the total order EFAST sensitivity indices can be obtained by adding the EFAST sensitivity indices from first order to 11th order:

$$E_j^{\mathrm{T}} = \sum_{j\in I} E_j + \sum_{j,k\in I, j<k} E_{jk} + \sum_{j,k,l\in I, j<k<l} E_{jkl} + \ldots \tag{19}$$

From the preceding equations, it is necessary to form triangular-shaped periodic sampling of X_i in the range of (0, 1) to calculate the EFAST sensitivity indices of X_i. Figure 11 shows the periodic sampling results of X_1 and X_2 in the range of (0, 1).

Because BPNN was trained with normalized parameters, the sampling results of X_i can be directly substituted into BPNN to calculate the EFAST sensitivity indices of 12 parameters, and EFAST sensitivity indices calculation results are shown in Table 6 and Fig. 12.

It can be seen from Table 6 and Fig. 12 that the sensitivity indices ranking results of 12 parameters calculated by the EFAST method are consistent with the results calculated by the Sobol' method, except for the total order sensitivity indices of X_9 and X_{12}, caused by calculation bias of Sobol' sensitivity indices. Also, the absolute error of the sensitivity indices of the corresponding parameters calculated by two methods is not more than 0.023, which shows the consistency of the calculation principle of the two variance-based GSA methods. Furthermore, in order to verify the reliability of the results of GSA based on the BPNN surrogate model, the results should be transferred back into conclusions on the thermal analysis model of the spectrometer system.

V. Verification of GSA Results

According to the total order sensitivity indices ranking results of 12 parameters calculated by the Sobol' method and EFAST method, by adjusting the value of sensitive and insensitive parameters in the finite element model of the spectrometer system respectively, the change amount and change rate of temperature T of the spectrometer frame under different conditions can be obtained, which can be used to verify the correctness of GSA results based on the BPNN surrogate

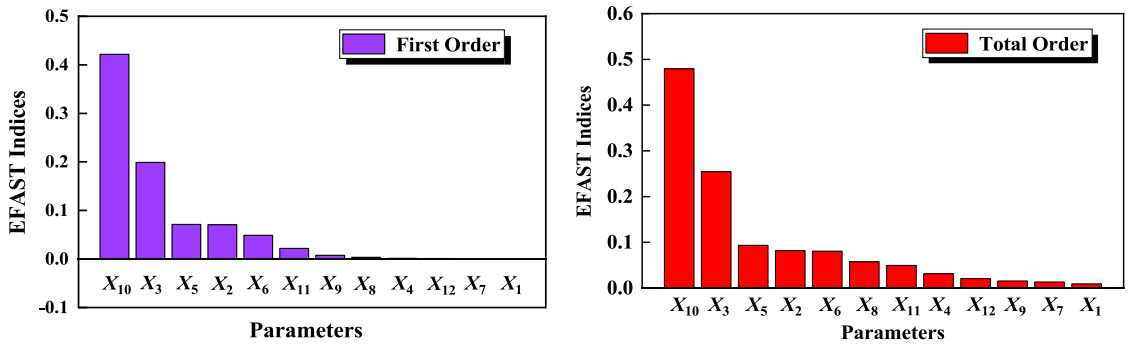

a) First Order b) Total Order

Fig. 12 First and total order EFAST indices of 12 parameters.

model. In this paper, satisfying the temperature index for the spectrometer frame under a summer solstice working condition was used as the criterion to adjust the parameter value, and the cooling rate of frame temperature T was used as the comparative index to verify the reliability of GSA results.

According to the temperature index of the frame temperature in Table 1 and the parameters of the summer solstice working condition in Table 3, in order to achieve the proposed thermal design index, it is necessary to improve the cooling capacity of the spectrometer system and reduce the impact of internal and external heat sources on temperature T. Table 7 shows the thermal control measures designed for 12 thermal design parameters and the optimal value of each parameter to meet the thermal design index.

In this paper, the thermal control measures numbered 2, 4, 5, and 9 and the thermal control measures numbered 1, 3, 6, 7, and 8 in Table 7 were taken as two groups to compare the cooling rate of temperature T by TMG finite element simulation. Numbers 2, 4, 5, and 9 are the thermal control measures corresponding to the parameters with higher sensitivity indices ranking, which are called "sensitive group"; 1, 3, 6, 7, and 8 are the thermal control measures corresponding to the parameters with lower sensitivity indices ranking, which are called "insensitive group." At the same time, the simulation results of taking all thermal control measures in Table 7 are referred to as "reference group." By substituting the different values of 12 parameters in 3 cases into the finite element model of the balloon-borne spectrometer system, the accuracy of the GSA results can be verified by comparing the cooling rate of temperature T and the satisfaction of the thermal

Table 7 Thermal control measures and corresponding parameters of spectrometer system

Number	Thermal control measures	Parameters
1	Using aluminum alloy as pod's material	$X_1 = 150\ \mathrm{W/(m \cdot K)}$
2	Spraying S781 white paint on all external surfaces of pod	$X_2 = 0.86, X_3 = 0.18$
3	Blackening internal surface of pod	$X_4 = 0.8$
4	Adding thermal insulation pad between CCD and frame of spectrometer	$X_5 = 50\ \mathrm{K/W}$
5	Adding thermal insulation pad between electrical box and pod	$X_6 = 50\ \mathrm{K/W}$
6	Dry contact at the connection of frame of spectrometer	$X_7 = 10\ \mathrm{K/W}$
7	Filling thermal conductive filler between spectrometer frame and surface of pod	$X_8 = 1000\ \mathrm{W/(m^2 \cdot K)}$
8	Connecting CCD and surface of pod with heat-conducting aluminum block	$X_9 = 1000\ \mathrm{W/(m^2 \cdot K)}$ $X_{10} = 8.5\ \mathrm{W/(m^2 \cdot K)}$
9	Improving the surface roughness of pod	$X_{11} = X_{12} = 7.5\ \mathrm{W/(m^2 \cdot K)}$

Table 8 Values of each parameter in three cases

Parameters	Sensitive group	Insensitive group	Reference group
$X_1/(\mathrm{W/m \cdot K})$	150	150	150
X_2	0.86	0.4	0.86
X_3	0.18	0.4	0.18
X_4	0.2	0.8	0.8
$X_5/\mathrm{K/W}$	50	5	50
$X_6/\mathrm{K/W}$	50	5	50
$X_7/\mathrm{K/W}$	10	10	10
$X_8/\mathrm{W/(m^2 \cdot K)}$	100	1000	1000
$X_9/\mathrm{W/(m^2 \cdot K)}$	100	1000	1000
$X_{10}/\mathrm{W/(m^2 \cdot K)}$	8.5	3	8.5
$X_{11}/\mathrm{W/(m^2 \cdot K)}$	7.5	3	7.5
$X_{12}/\mathrm{W/(m^2 \cdot K)}$	7.5	3	7.5

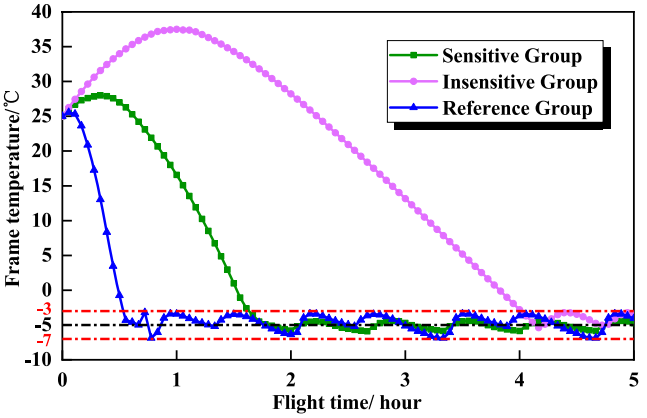

Fig. 13 Temperature curve of spectrometer frame in three cases.

design index in three cases. Table 8 shows the values of each parameter in three cases.

According to the working-condition parameters in Table 3, after adjusting the simulation time to 5 h and setting the active thermal control measures working for the whole process, the parameter values in Table 8 were substituted into the finite element model, and the time-dependent curves of the frame temperature T of three groups were obtained, as shown in Fig. 13.

It can be seen from Fig. 13 that the cooling rate of temperature T of the sensitive group (mean value 0.43°C/ min) is higher than that of the insensitive group (mean value 0.23°C/ min). In addition, under the condition of adopting the thermal control measures of the sensitive group, the simulated frame temperature T meets the thermal design index of maintaining -5 ± 2°C for more than 3 h, reaching 3.4 h, whereas the thermal control measures of the sensitive group cannot meet the thermal control index, and the time of maintaining the temperature level is not more than 1 h. The comparison results demonstrate that the influence of parameters in the sensitive group on the temperature T is greater than that of parameters in the insensitive group, which indicates the correctness of GSA results based on the BPNN surrogate model. Furthermore, the cooling rate of temperature T of the reference group (mean value 0.89°C/ min) is higher than that of the sensitive group, which is caused by the effect of the parameter in the insensitive group and the joint coupling effect of 12 parameters on temperature T. The thermal control measures of the reference group can better meet the proposed thermal design index. However, from the perspective of resource saving, the thermal control measures of the sensitive group can meet the temperature index more economically and with more energy saving.

After GSA results were verified, this paper also introduced the Spearman rank correlation coefficient (SRCC) formula [24], which is often used in thermal analysis model modification, to calculate the monotonic goodness-of-fit of 12 parameters to the temperature T to express the influence of each parameter on T. Different from the sensitivity indices of the Sobol' or EFAST method, the SRCC formula can only calculate the correlation degree between parameters and temperature T. Although the calculation results can reflect the influence of parameters on model output to some extent, it does not belong to the sensitivity category in mathematical sense. However, due to the fast calculation speed of SRCC, it is widely used in the rough modification of a thermal analysis model to find the most important parameters that affect the output of the model. According to the data set in Table 4, the monotonic goodness-of-fit values of 12 parameters were calculated by using the SRCC formula, and the results were compared with the total order sensitivity indices calculated by the Sobol' and EFAST methods. The comparison results are shown in Fig. 14.

In order to make a more intuitive comparison, the results of the SRCC formula were squared to make the results of the three methods in the same scales. From the comparison results in Fig. 14, it can be seen that the ranking results of parameters' monotonic goodness-of-fit calculated by the SRCC formula are inconsistent with 12 parameters'

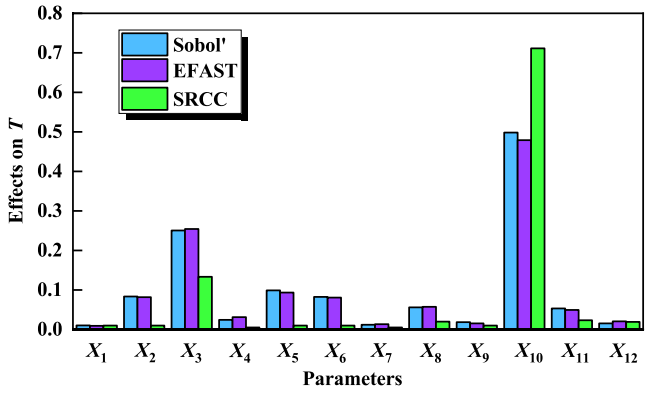

Fig. 14 Comparison of parameter SA results obtained by three methods.

sensitivity indices ranking results of the Sobol' and EFAST method, except for X_{10} and X_3. Morover, the gap of the results calculated by the three methods is actually caused by the nonmonotonic part of the model. The comparison results firstly indicate that the monotonic goodness-of-fit of the sensitive parameters calculated by the SRCC formula can be used to express the influence of parameters on the model output. Secondly, the SRCC formula cannot calculate the influence of parameters on the nonlinear part of the model (higher order response), making it unable to distinguish the actual sensitivity indices of parameters with low sensitivity. Finally, the monotonic goodness-of-fit calculated by the SRCC formula does not include the influence of multiparameter coupling on the model output, and the calculation error of the SRCC formula is large when calculating the actual influence of 12 parameters on temperature T. Therefore, the SRCC formula is not suitable for other parameter SA tasks except the case where only the parameters that have the most important influence on the model output need to be studied. In addition, the time spent by the three methods in calculating the sensitivity of parameters was compared, and the comparison results are shown in Table 9.

The data given in Table 9 shows that the Sobol' method takes the longest time, 3440.238 s, to calculate the global sensitivity indices of 12 parameters, and the time is mainly spent on calculation of parameter sensitivity indices. This is because a large number of parameter samples are needed to ensure the convergence of calculation results when the Sobol' method is used to calculate the sensitivity indices of parameters. In this paper, 280,000 sets of sampling data were used for the calculation of Sobol' sensitivity indices of 12 parameters, resulting in the limited calculation speed of the Sobol' method. Different from the Sobol' method, the EFAST method can obtain the convergent parameter sensitivity indices without a large number of parameter sampling. Therefore, the calculation time of the EFAST method to calculate the first and total order EFAST indices of 12 parameters in this paper is only 70.94 s, much shorter than Sobol's. Additionally, because of the simple calculation principle and few computational procedures, the calculation speed of the monotonic goodness-of-fit of 12 parameters by using the SRCC formula is the fastest, with only 3.002 s needed. However, in terms of the reliability of the calculation results, the calculation results of the EFAST method are more reliable than those of SRCC, so that calculation time of 70.94 s is acceptable.

Furthermore, this paper also compared the time of simulation between the BPNN metamodel and finite element model. The results indicate that the average single simulation time of the finite element model is 423.6 s, whereas the time of the BPNN metamodel is 0.0122 s, which is much lower than that of the finite element model. In this study, the calculation of Sobol' indices called BPNN for 280,000 times, which took 3425 s, whereas the finite element model only simulated 200 times, taking more than 23 h. Therefore, the speed advantage of GSA based on the metamodel is obvious. In addition, in this paper, the computing speed of GSA based on the BPNN surrogate model is also limited by the computing resources (Intel Core i5-4200 CPU, 12 GB RAM), which leads to the longer calculation time of sensitivity indices. With the further improvement of computing resources, the calculation time of GSA will be further shortened, further promoting the application of GSA in thermal analysis tasks.

Table 9 Comparison of three methods in calculating time

Process	Sobol'	EFAST	SRCC
Data preprocessing	1.998 s	1.998 s	1.998 s
Training of surrogate model	12.583 s	12.583 s	None
Calculation of Parameter sensitivity indices	3425.657 s	56.359 s	1.004 s
Total time cost	3440.238 s	70.94 s	3.002 s

VI. Conclusions

In the current research of GSA for thermal design parameters of an optical remote sensor, it is difficult to directly establish the display function between target temperature and parameters, which limits the application of various GSA methods. In this paper, the variance-based GSA methods, Sobol' method and EFAST method, based on the BPNN surrogate model, were introduced to calculate the first and total order sensitivity indices of 12 parameters to the temperature T of the spectrometer frame, to study the influence of parameters on temperature T in a balloon-borne spectrometer system. Then, based on the ranking results of sensitivity indices of 12 parameters, the thermal control measures are designed for sensitive parameters and insensitive parameters respectively, and the cooling rate and satisfaction of the temperature index of temperature T under the two conditions are obtained by finite element simulation in I-DEAS/TMG. The simulation results indicate that the cooling rate of the sensitive group is higher than that of the insensitive group, and thermal control measures of the sensitive group meet the requirements of maintaining temperature T at -5 ± 2°C for more than 3 h, whereas the thermal control measures of the insensitive group cannot meet the index, which shows the correctness and reliability of GSA results based on BPNN. At the end of this paper, the monotonic goodness-of-fit of 12 parameters calculated by the SRCC formula, which is commonly used in thermal analysis model modification, was compared with sensitivity indices calculated by the Sobol' method and EFAST method. The comparison results show that although the calculation speed of the SRCC formula is fastest among the three methods, the calculation results of this formula do not belong to the category of sensitivity indices and they lack reliability. Different from this, the EFAST method based on BPNN has greater advantages in the reliability of calculation results and in the speed of the computation process, which is conducive to the promotion of surrogate-based GSA in thermal analysis tasks. Moreover, the influence of a BPNN training error on the calculation results of sensitivity indices is beyond the scope of this paper and will be studied in a consecutive paper.

Acknowledgment

This work received funding from the National Key Research & Development Program of China, 2018YFB0504800 (2018YFB0504801) is a project number.

References

[1] Borgonovo, E., and Plischke, E., "Sensitivity Analysis: A Review of Recent Advances," *European Journal of Operational Research*, Vol. 248, No. 3, 2016, pp. 869–887. https://doi.org/10.1016/j.ejor.2015.06.032

[2] Saltelli, A., Ratto, M., Tarantola, S., Campolongo, F., et al., "Sensitivity Analysis Practices: Strategies for Model-Based Inference," *Reliability Engineering & System Safety*, Vol. 91, Nos. 10–11, 2006, pp. 1109–1125. https://doi.org/10.1016/j.ress.2005.11.014

[3] Saltelli, A., Ratto, M., Andres, T., Campolongo, F., Cariboni, J., Gatelli, D., Saisana, M., and Tarantola, S., *Global Sensitivity Analysis: The Primer*, Wiley, Hoboken, NJ, 2008, pp. 1–9, Chap. 1.

[4] Scire, J. J., Jr., Dryer, F. L., and Yetter, R. A., "Comparison of Global and Local Sensitivity Techniques for Rate Constants Determined Using Complex Reaction Mechanisms," *International Journal of Chemical Kinetics*, Vol. 33, No. 12, 2001, pp. 784–802. https://doi.org/10.1002/kin.10001

[5] Han, C. Y., You, J. H., Lee, K. H., Kim, H. K., and Lee, S. N., "Sensitivity Analyses of Satellite Propulsion Components with Their Thermal Modelling," *Advances in Space Research*, Vol. 47, No. 3, 2011, pp. 466–479. https://doi.org/10.1016/j.asr.2010.09.018

[6] Guo, L., Wu, Q.-W., and Yan, C.-X., "Sensitivity of Thermal Design Parameters for Space Spectral Imaging Apparatus," *Guangxue Jingmi Gongcheng (Optics and Precision Engineering)*, Vol. 20, No. 6, 2012, pp. 1208–1217.

[7] Guo, L., Wu, Q.-W., and Yan, C.-X., "Sensitivity Analysis of Thermal Design Parameters for Focal Plane Assembly in a Space Spectral Imaging Instrument," *Heat and Mass Transfer*, Vol. 49, No. 3, 2013, pp. 299–308. https://doi.org/10.1007/s00231-012-1086-7

[8] McMenamin, C. B., "Application of Bayesian-Based Uncertainty and Global Sensitivity Analyses to Spacecraft Thermal Design," Ph.D. Thesis, Massachusetts Institute of Technology, Cambridge, MA, 2016.

[9] Blatman, G., and Sudret, B., "A Comparison of Three Metamodel-Based Methods for Global Sensitivity Analysis: GP Modelling, HDMR and LAR-gPC," *Procedia Social & Behavioral Sciences*, Vol. 2, No. 6, 2010, pp. 7613–7614. https://doi.org/10.1016/j.sbspro.2010.05.143

[10] Ge, Q., Ciuffo, B., and Menendez, M., "Combining Screening and Metamodel-Based Methods: An Efficient Sequential Approach for the Sensitivity Analysis of Model Outputs," *Reliability Engineering & System Safety*, Vol. 134, 2015, pp. 334–344. https://doi.org/10.1016/j.ress.2014.08.009

[11] Jin, R., Chen, W., and Sudjianto, A., "Analytical Metamodel-Based Global Sensitivity Analysis and Uncertainty Propagation for Robust Design," *SAE Transactions*, Vol. 38, No. 4, 2004, pp. 121–128. https://doi.org/10.4271/2004-01-0429

[12] Saltelli, A., Annoni, P., Azzini, I., Campolongo, F., Ratto, M., and Tarantola, S., "Variance Based Sensitivity Analysis of Model Output. Design and Estimator for the Total Sensitivity Index," *Computer Physics Communications*, Vol. 181, No. 2, 2010, pp. 259–270. https://doi.org/10.1016/j.cpc.2009.09.018

[13] Giltnore, D. G. (ed.), *Spacecraft Thermal Control Handbook Volume 1: Fundamental Technologies*, 2nd ed., The Aerospace Press, 2002, pp. 21–36, Chap. 2.

[14] Li, S., Yang, B., and Qi, F., "Accelerate Global Sensitivity Analysis Using Artificial Neural Network Algorithm: Case Studies for Combustion Kinetic Model," *Combustion and Flame*, Vol. 168, 2016, pp. 53–64. https://doi.org/10.1016/j.combustflame.2016.03.028

[15] Wang, C. Y., Zhang, F., and Han, W. D., "Sensitivity Analysis of Slope Stability Influence Factors Based on BP Neural Network," *Advanced Materials Research*, Vol. 1010, 2014, pp. 1544–1547. https://doi.org/10.4028/www.scientific.net/amr.1010-1012.1544

[16] Wythoff, B. J., "Backpropagation Neural Networks: A Tutorial," *Chemometrics and Intelligent Laboratory Systems*, Vol. 18, No. 2, 1993, pp. 115–155. https://doi.org/10.1016/0169-7439(93)80052-j

[17] Primadusi, U., Cahyadi, A. I., Prasetyo, D., and Wahyunggoro, O., "Backpropagation Neural Network Models for $LiFePO_4$ Battery," *AIP Conference Proceedings*, Vol. 1755, No. 1, 2016, Paper 090009. https://doi.org/10.1063/1.4958527

[18] Bhatikar, S. R., Mahajan, R. L., Wipke, K., and Johnson, V., "Artificial Neural Network Based Energy Storage System Modeling for Hybrid Electric Vehicles," SAE Technical Paper, 2000, pp. 2–3. https://doi.org/10.2172/935117

[19] Zhao, Z., Xin, H., Ren, Y., and Guo, X., "Application and Comparison of BP Neural Network Algorithm in MATLAB," *2010 International Conference on Measuring Technology and Mechatronics Automation*, Vol. 1, IEEE Computer Soc., 2010, pp. 590–593. https://doi.org/10.1109/ICMTMA.2010.492

[20] Sobol', I. M., "Sensitivity Estimates for Nonlinear Mathematical Models," *Mathematical Modelling and Computational Experiments*, Vol. 1, No. 4, 1993, pp. 407–414.

[21] Nossent, J., Elsen, P., and Bauwens, W., "Sobol' Sensitivity Analysis of a Complex Environmental Model," *Environmental Modelling & Software*, Vol. 26, No. 12, 2011, pp. 1515–1525. https://doi.org/10.1016/j.envsoft.2011.08.010

[22] Saltelli, A., and Bolado, R., "An Alternative Way to Compute Fourier Amplitude Sensitivity Test (FAST)," *Computational Statistics & Data Analysis*, Vol. 26, No. 4, 1998, pp. 445–460. https://doi.org/10.1016/S0167-9473(97)00043-1

[23] Plischke, E., "An Effective Algorithm for Computing Global Sensitivity Indices (EASI)," *Reliability Engineering & System Safety*, Vol. 95, No. 4, 2010, pp. 354–360. https://doi.org/10.1016/j.ress.2009.11.005

[24] Shuming, G., and Hailing, Z., *Applied Statistics*, 3rd ed., China Water Power Press, Beijing, 2010, pp. 250–251, Chap. 3.